

Chapter 4

Semiconductor Detector-Based Scanners for Nuclear Medicine

Wataru Takeuchi, Atsuro Suzuki, Yuichiro Ueno, Tohru Shiga, Kenji Hirata, Shozo Okamoto, Songji Zhao, Yuji Kuge, Naoki Kubo, Kentaro Kobayashi, Shiro Watanabe, Keiji Kobashi, Kikuo Umegaki, and Nagara Tamaki

Abstract Semiconductor detectors have the potential to improve the quantitative accuracy of nuclear medicine imaging with their better energy and intrinsic spatial resolutions than those of conventional scintillator-based detectors. The fine energy resolution leads to a better image contrast due to better scatter rejection. The fine intrinsic spatial resolution due to a pixelated structure leads to a better image contrast and lower partial volume effect. Their pixelated structures also improve the count-rate capability. The authors developed CdTe semiconductor detector-based positron emission tomography (CdTe-PET) and single-photon emission computed tomography (CdTe-SPECT) in order to test the potential of using semiconductor detectors in nuclear medicine. The physical performances of both systems were measured in several phantom experiments. The capability of using CdTe-PET

W. Takeuchi (✉) • A. Suzuki • K. Kobashi
Research and Development Group, Hitachi Ltd., 1-280, Higashi-Koigakubo Kokubunji-shi,
Tokyo 185-8601, Japan
e-mail: wataru.takeuchi.rg@hitachi.com

Y. Ueno
Research and Development Group, Hitachi Ltd., 1-280, Higashi-Koigakubo Kokubunji-shi,
Tokyo 185-8601, Japan

Faculty of Engineering, Hokkaido University, Sapporo, Japan

T. Shiga • N. Tamaki
Department of Nuclear Medicine, Graduate School of Medicine, Hokkaido University,
Sapporo, Japan

K. Hirata • S. Okamoto • S. Zhao • K. Kobayashi • S. Watanabe
Graduate School of Medicine, Hokkaido University, Sapporo, Japan

Y. Kuge
Central Institute of Isotope Science, Hokkaido University Department of Integrated Molecular
Imaging, Graduate School of Medicine, Hokkaido University, Sapporo, Japan

N. Kubo
Office of Health and Safety, Hokkaido University, Sapporo, Hokkaido, Japan

K. Umegaki
Faculty of Engineering, Hokkaido University, Sapporo, Japan

to measure the metabolic distribution of tumors was evaluated through scans of cancer patients and rat tumor models. The feasibility of using CdTe-SPECT for simultaneous dual-radionuclide imaging was evaluated through scans of phantoms and healthy volunteers. The results suggest that the prototype CdTe-PET can identify intratumoral metabolic heterogeneous distribution and that CdTe-SPECT can accurately acquire dual-radionuclide images simultaneously. Although there are still problems to be solved, semiconductor detectors will play significant roles in the future of nuclear medicine.

Keywords Semiconductor detector • Solid-state detector • CdTe • Intratumoral heterogeneity • Dual radionuclide

4.1 Introduction

Nuclear medicine plays a significant role in diagnosis, treatment planning, and treatment response evaluation. In particular, in oncology, biological imaging by positron emission tomography (PET) permits not only tumor detection but also gross tumor delineation and identification of biological heterogeneities [1, 2]. In the delineation of tumor boundaries by PET, achieving a good spatial resolution and quantitative accuracy are physical imaging concerns. The spatial resolution of the current PET images as used in clinical practice is 7–9 mm after reconstruction with many systems. The achievable spatial resolution depends primarily on the size of the detector elements. The typical PET scanner used in current clinical study is comprised of scintillation detectors 4×4 mm in size.

In nuclear cardiology and brain nuclear medicine, functional imaging by PET and single-photon emission computed tomography (SPECT) can measure the functional state of the myocardium and brain. Unlike PET, SPECT has the potential to enable simultaneous multi-radionuclide imaging. The scanning of multi-radionuclide pharmaceuticals will enable various kinds of functional images to be obtained without position error or time difference. The recent development of several cardiac SPECT systems that use solid-state detectors with a fine energy resolution [3–5] has led to simultaneous multi-radionuclide imaging recapturing the spotlight. A number of simultaneous multi-radionuclide imaging studies have been reported, especially for myocardial perfusion diagnosis [4, 5]. To enable accurate simultaneous multi-radionuclide imaging, a detector with a good energy resolution is necessary. In addition, improving the sensitivity of gamma-ray detection is also important for realizing simultaneous multi-radionuclide imaging with an appropriate dose of radiopharmaceuticals.

As mentioned above, the performance of nuclear medicine imaging depends on spatial resolution, energy resolution, and sensitivity. Semiconductor detectors, e.g., CdZnTe or CdTe detectors, provide improved energy resolution due to the direct conversion of gamma rays to charge carriers. This fine resolution leads to a better image contrast due to better scatter rejection. Semiconductor detectors also easily provide a pixelated structure that improves the count-rate capability and intrinsic spatial resolution. Flexibility in both sizing and a fine arrangement of semiconductor

detectors is expected not only to improve the spatial resolution but also to obtain depth-of-interaction (DOI) information in PET and pixel-of-interaction in SPECT when the multidetector pixels are placed within each collimator hole. A high energy resolution is expected to reduce scattered components in detected signals and to improve the quantitative accuracy of the reconstructed images. These features of semiconductor detectors may lead to improved PET and SPECT images. The authors previously developed CdTe semiconductor detector-based PET (CdTe-PET) [1, 2] and SPECT (CdTe-SPECT) [6, 7]. The physical and clinical performances of the systems were evaluated through phantom, animal, and clinical studies.

4.2 Materials and Methods

4.2.1 Development and Performance Evaluation of Prototype CdTe-PET

4.2.1.1 Outline of CdTe-PET and Its Parameter Settings

CdTe-PET is a prototype semiconductor PET scanner for human brain imaging. This scanner is described in detail in a previous report [1]. In brief, the scanner uses CdTe detectors for dedicated three-dimensional emission scanning. It has a patient port with a diameter of 350 mm, a transaxial FOV of 310 mm, and an axial FOV of 250 mm. The size of a detector is $1.0 \times 4.0 \times 7.5$ mm. The detector channel is composed of two CdTe elements in the radial direction and two CdTe elements in the tangential direction. To utilize the depth-of-interaction (DOI) technique, three detector channels (six detectors) in the tangential direction are used. The transverse and axial spatial resolutions near the center are 2.3 and 5.1 mm, respectively. The energy resolution is 4.1 % at 511 keV (FWHM), which is superior to that of available scintillation detectors, e.g., 10–20 %. The long-term stability of the energy resolution of the CdTe detectors was assured by periodically resetting the bias [8]. No significant variances in the spectral peak position and energy resolution of the CdTe detectors were observed for over a year [9].

The energy of detected gamma rays is recorded in list-mode data. This data contains the energy information of two gamma rays in the coincidence detection. The size of an energy bin is 4 keV. Two energy windows, described below, were used. One energy window (390–540 keV) was used as a wide energy window (WEW), and another (494–540 keV) was used as a photopeak energy window (PEW). Sinogram data using both WEW and PEW were made by sorting the list-mode data by recorded energy. For all measured sinogram data and energy spectra, random coincidences were removed by using the delayed coincidence subtraction technique. The size of the sinogram data is 256 in the radial direction, 256 in the angular direction, 87 in the axial direction, and 44 in the oblique angular direction, i.e., ring difference. The matrix size of the reconstructed images is $256 \times 256 \times 87$ with voxels of $1.21 \times 1.21 \times 2.8$ mm.

To bring out the potential of CdTe detectors in human imaging, the main challenge to be solved is sensitivity. The effective atomic number of the CdTe is smaller than the scintillation detectors of the current PET scanner. The crystal size is also smaller than those detectors. To overcome the sensitivity problem, the following improvements were made.

To improve sensitivity, a novel signal processing method was developed [1]. The effective atomic number of the CdTe is 50, so the whole absorption rate of the 511-keV gamma ray is smaller than the current scintillation detectors, and a considerable amount of scattered gamma rays are generated and absorbed in nearby detectors. In the improved signal processing method, when the sum of the energy of two gamma rays detected in a neighborhood channel in a limited time window (64 ns) is around 511 keV, the record of the gamma rays detected at the opposing detector unit in the coincidence time window (14 ns) is checked for the coincidence detection. With this signal processing, the detector of our system is considered to be a continuous mass of CdTe from the viewpoint of sensitivity, although the position is determined digitally.

4.2.1.2 Image Reconstruction Method

A reconstruction system of the developed scanner coped with the sensitivity problem, avoiding unexpected statistical fluctuation in reconstructed images. To enable high-resolution imaging with a low amount of statistical data, we developed a reconstruction method that could suppress statistical noise without degrading the spatial resolution [1, 10]. The method is based on maximum a posteriori (MAP) [11] with median root prior (MRP) [12] and uses a resolution recovery technique [13, 14]. The method also uses an attenuation and normalization weighting technique. MRP assumes only local monotony and does not need any anatomical information such as MRI or CT images. MRP is also known as an effectual prior for reducing noise and preserving edge. Because of various incident angles and distances to detectors, reconstructed point source images blur into various shapes. To correct the point spread function (PSF), a 3-D image-space convolution technique was used [13]. The Gaussian kernel represents the PSF. The algorithm of the reconstruction method, named “point spread function correction with median root prior” (PSC-MRP), is shown in Eq. (4.1):

$$\lambda_j^{k+1} = \frac{\lambda_j^k}{\left(1 + \beta \frac{\lambda_j^k - M_j}{M_j}\right) \cdot \left(\sum_i p_{ij} a_j n_j\right) \otimes G} \left(\sum_i p_{ij} \frac{y_i}{\sum_j p_{ij'} (\lambda_j^k \otimes G)} \right) \otimes G \quad (4.1)$$

λ : pixelvalue ($j = \text{index}, k = \text{iteration}$)
 y : observed data ($i = \text{index}$)
 p : probability-matrix
 a : attenuation-matrix
 n : normalization-matrix
 M : median of the neighbourhood
 G : Gaussian-Kernel (PSF)
 β : prior strength

The value y is measured data, and λ is emission image. The matrices p , a , and n represent probability (geometrical sensitivity), attenuation, and normalization (sensitivity of each detector), respectively. The value k is the number of iterations, and i and j are index numbers. The value β controls the effect of reducing noise, and M is a median of neighbor ($3 \times 3 \times 3$) voxels' values. The Gaussian kernel G represents the PSF. The PSFs were measured for a point source at different positions in a portion of the field of view. The G was parameterized to correct for point source location and to smooth for projection noise. When β is zero and G is not used, the reconstruction method equals attenuation and normalization weighted OSEM (ANW-OSEM) [15]. The numbers of subsets and iterations were 8 and 5, respectively.

4.2.1.3 Physical Performance Measurement

In accordance with the NEMA NU2-1994 standards [16], a count-rate performance experiment was conducted with CdTe-PET. In this evaluation, two energy windows (WEW and PEW described above) were used. The count-rate performance of CdTe-PET was measured with a standard 20-cm-inner-diameter, 20-cm-long phantom filled with water that contained a 3.7-kBq/cm³ F-18 solution. The phantom was placed at the center of the FOV and scanned over ten half-lives. The performance was evaluated in WEW and PEW settings. The noise equivalent count rate (NEC2R) was calculated by $NEC2R = T^2 / (T + S + 2 \cdot R)$ from the true (T) rate, scattered (S) rate, and random (R) rate. The random rate was multiplied by a factor of two because the random rate was evaluated by acquiring events in a delayed time window. The sensitivity of the scanner was also evaluated using the measurement data of count-rate performance.

4.2.1.4 Image Quality Evaluation

To evaluate the image quality of CdTe-PET with its energy window set to PEW, two kinds of experiments and studies, described below, were conducted.

Hoffman Phantom

A Hoffman phantom (filled with 9.1 kBq/ml F-18 solution) simulated the human brain was scanned for 10 min so as to equalize the measured count with the clinical situation. The data was reconstructed by (a) ANW-OSEM, (b) ANW-OSEM with post-reconstruction Gaussian filter (4-mm FWHM), and (c) PSC-MAP $\beta = 0.05$. The three images were compared visually.

Preclinical Evaluation with Rat Tumor Model

To evaluate the feasibility of visualizing intratumoral heterogeneity, a preclinical study using a rat tumor model was conducted. All animal care and experimental procedures were performed with the approval of the Laboratory Animal Care and Use Committee of Hokkaido University. Eight-week-old male Wistar-King-Aptekman/hok (WKAH) rats (Japan SLC, Inc.) were inoculated with a suspension of allogenic rat glioma cells (C6, 2×10^6 cells/0.2 ml) into the left calf muscle to generate glioma rat models. The rats were allowed free access to water and laboratory chow until the day before the experiment. When the tumors were 1–2 cm in diameter, the rats were fasted overnight. Under diethyl ether anesthesia, 200 kBq/g body weight of F-18-fluorodeoxyglucose (FDG) was intravenously injected into each rat. Fifty minutes after the injection of FDG, the rats were anesthetized with pentobarbital (50 mg/kg body weight, intraperitoneally). One hour after the FDG injection, each rat was scanned by CdTe-PET for 1 min. Then, images were reconstructed by PSC-MAP ($\beta = 0.05$). Four hours after the FDG injection, the rats were euthanized under deep pentobarbital anesthesia. The animals were sacrificed, and the whole tumors were quickly excised. Then, the excised tumors were frozen in isopentane/dry ice. The frozen tumor tissues were sectioned into slices for autoradiographic (ARG) imaging. The thickness of the sectioned slices was 0.15 mm. The number of slices was about 19. All of the sectioned slices were exposed to phosphor imaging plates (BAS-SR 2025, Fuji Photo Film Co., Ltd.) together with a set of calibrated standards. The autoradiographic exposure was performed for 12 h to detect the radioactivity of FDG. After the exposure, the imaging plates were scanned with a Fuji Bio-imaging Analyzer BAS-5000, and the units of the images were converted into a unit of Bq/ml by house-made software. All of the sectioned slices were integrated into a 3-D volume by using a slice-by-slice image registration technique. Then, the integrated 3-D ARG and PET images were compared.

Clinical Evaluation

As was previously reported [1, 2], patients with brain tumor or nasopharyngeal cancer injected FDG (340 MBq ca.) were scanned by CdTe-PET for 30 min. Then, images were reconstructed by PSC-MAP ($\beta = 0.05$). The patient volunteers gave

written, informed consent in accordance with the Helsinki II Declaration. The study was approved by the ethics committees of both the Hokkaido University Graduate School of Medicine and Hitachi, Ltd. The capability of using CdTe-PET to measure the metabolic distribution of tumor was evaluated.

4.2.2 Development and Performance Evaluation of Prototype CdTe-SPECT

4.2.2.1 Outline of CdTe-SPECT

CdTe-SPECT is a prototype semiconductor SPECT system for human brain imaging. This system is described in detail in previous reports [6, 7]. In brief, CdTe-SPECT includes two detector heads. Each head consists of 192×96 detector pixels with a pitch of 1.4 mm, so the field of view of the detector head is 268×134 mm (tangential \times axial). The size of each detector pixel is $1.2 \times 1.4 \times 5$ mm. The intrinsic energy resolution (FWHM) of the CdTe detector is 6.6 % at 140.5 keV, and the count-rate linearity is maintained at 200 kcps per head and under [9]. For high-sensitivity imaging, a wide aperture parallel-hole collimator (Fig. 4.1), which we call the “4-pixel matched collimator” (4-PMC), was previously developed [6, 7]. The hole size of the 4-PMC is matched to four detector pixels, that is, there are four (2×2) pixels per collimator hole. By contrast, the hole size of the standard parallel-hole collimator [9] is matched to one detector pixel, that is, a 1-pixel matched collimator (1-PMC). The specifications of both collimators are shown in Table 4.1. 4-PMC was designed to improve the sensitivity and spatial resolution in clinical SPECT imaging compared with 1-PMC. The sensitivities of 1-PMC and 4-PMC were 70 and 220 cps/MBq/head, respectively [7]. Therefore, 4-PMC has three times the sensitivity of 1-PMC. The rotation radius of the detector head is set to 130 mm for brain scans. In SPECT acquisition, each detector head is rotated by 360° over 3 min.

Fig. 4.1 Geometry of 4-PMC

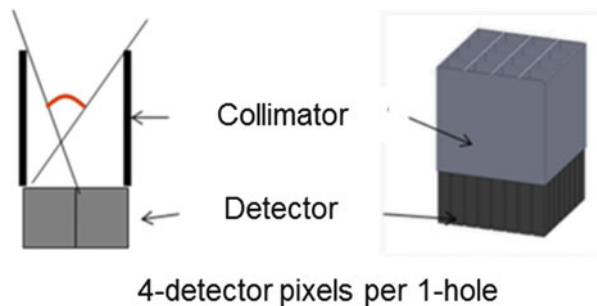


Table 4.1 Collimator specifications

Type	Hole pitch (mm)	Hole size (mm)	Hole length (mm)	Sensitivity (cps/MBq/head)
1-PMC	1.4	1.12	20.0	70
4-PMC	2.8	2.40	26.0	220

4.2.2.2 Image Reconstruction Method

The ordered subset expectation maximization (OSEM) (Hudson and Larkin 1994) including PSF and attenuation correction was used. The PSF of each collimator type was obtained by ray-tracing simulation [6, 7]. The attenuation factor of the gamma rays in a subject was approximated by an exponential function of the line integral from an image pixel to a detector pixel in an attenuation map. The projection image matrix size (tangential \times axial) was 256×96 (pixel size = 1.4×1.4 mm). The number of projection images was 120 over 360° . The reconstructed image matrix size ($x \times y \times z$) was $256 \times 256 \times 96$ (pixel size = $1.4 \times 1.4 \times 1.4$ mm). The numbers of subsets and iterations were 30 and 20, respectively. The reconstructed images were smoothed with a 14-mm FWHM Gaussian filter.

4.2.2.3 Performance Evaluation in Phantom Experiment and Clinical Study

Dual-Radionuclide Character-Shape Phantom

A character-shape dual-radionuclide phantom, which has three kinds of radioactivity, was scanned (Fig. 4.2). The activities are shown in Table 4.2. The photopeak energy windows for Tc-99m (141 keV) and I-123 (159 keV) were 130–148 keV and 155–170 keV, respectively. An energy window-based scatter correction based on the triple energy window (TEW) method [17] was used. The measured energy spectrum and reconstructed images were evaluated.

Simultaneous Dual-Radionuclide Human Brain Study

A healthy volunteer was injected with Tc-99m HAS-D and I-123 IMP and then scanned by CdTe-SPECT for 21 min as a simultaneous dual-radionuclide brain study. The healthy volunteer gave written, informed consent in accordance with the Helsinki II Declaration. The study was approved by the ethics committees of both the Hokkaido University Graduate School of Medicine and Hitachi, Ltd. The

Fig. 4.2 Dual-radionuclide character-shape phantom

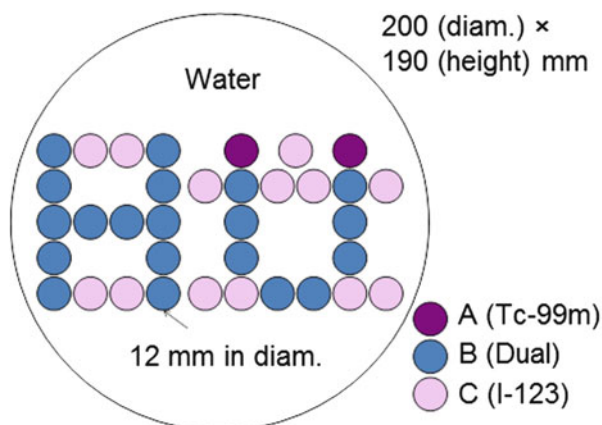


Table 4.2 Radioactivities of dual-radionuclide character-shape phantom

Kinds of vial	Tc-99m (kBq/ml)	I-123 (kBq/ml)
A (Tc-99m)	44.6	0
B (Dual)	49.3	115.5
C (I-123)	0	101

feasibility of using CdTe-SPECT for simultaneous dual-radionuclide study was evaluated.

4.3 Results and Discussion

4.3.1 Performance Evaluation of CdTe-PET by Phantom Experiment and Clinical Study

4.3.1.1 Physical Performance of CdTe-PET

Figure 4.3 shows the result of the count-rate performance examination. The left vertical axis is the count rate of “true” and “random.” The right vertical axis is the noise equivalent count rate (NEC2R). The horizontal axis is the activity of the cylinder phantom. Table 4.3 shows the results for sensitivity, NECR, and scatter fraction. The sensitivity was 22.0 and 8.5 kcps/(kBq/ml) in WEW and PEW, respectively. The NECR at 7.4 kBq/ml was 45 and 25 kcps in WEW and PEW, respectively. The scatter fraction was 39 and 12 % in WEW and PEW, respectively. Comparing PEW with WEW, although the sensitivity was less than a half, the NECR was more than a half. The scatter fraction for PEW was less than a third of that for WEW.

Fig. 4.3 Count-rate performance

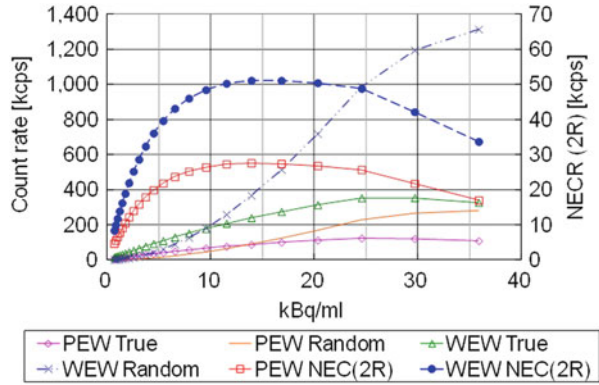


Table 4.3 Count-rate performances in each energy window

Energy window	WEW	PEW
Sensitivity [kcps/(kBq/ml)]	22.0	8.5
Peak NECR [kcps]	51	28
NECR at 3.7 kBq/ml [kcps]	32	18
NECR at 7.4 kBq/ml [kcps]	45	25
Scatter fraction [%]	39	12

4.3.1.2 Image Quality of CdTe-PET

Hoffman Phantom

Shown in Fig. 4.4 are images reconstructed by (a) ANW-OSEM, (b) ANW-OSEM with a Gaussian filter (4-mm FWHM), and (c) PSC-MAP $\beta=0.05$. Even with filtering, images reconstructed by ANW-OSEM had speckle noise. The PSC-MAP image was not speckled and not blurred. Therefore, the edge between gray matter and white matter in the PSC-MAP image was well defined.

Preclinical Evaluation with Rat Tumor Model

The diameter of each tumor was ca. 16 mm. A 3-D ARG volume made by integrating 19 slices is shown in Fig. 4.5. The heterogeneous intratumoral FDG distribution in each tumor was visualized by both CdTe-PET and ARG (Figs. 4.5 and 4.6). CdTe-PET images were visually consistent with ARG (Fig. 4.6).

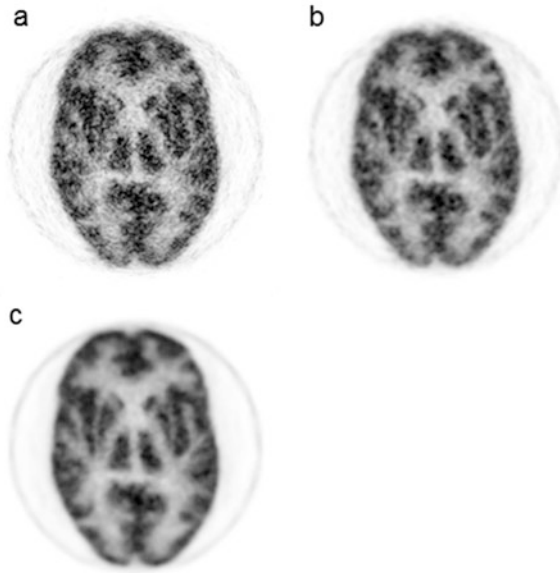


Fig. 4.4 Reconstructed image of Hoffman phantom. (a) ANW-OSEM, (b) ANW-OSEM+ Gaussian filter, and (c) PSC-MAP ($b=0.05$)

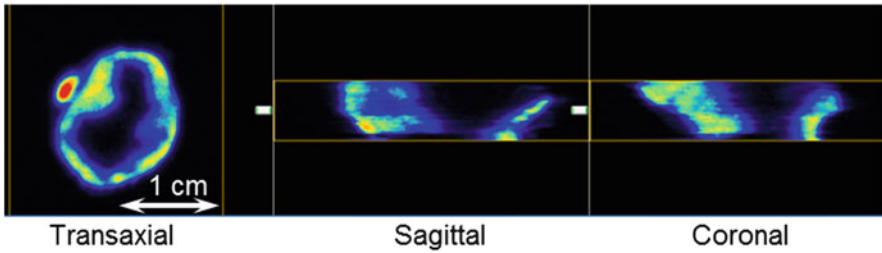


Fig. 4.5 Integrated 3-D ARG volume

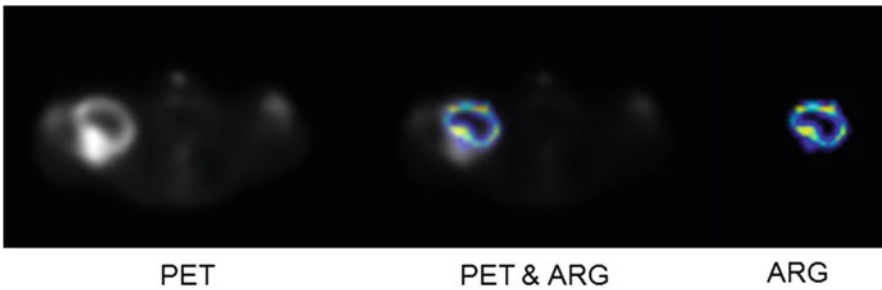
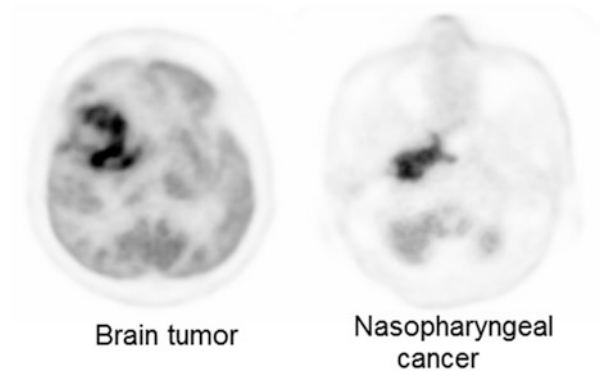


Fig. 4.6 Comparison of ARG and PET images. “PET+ARG” shows image fused by image registration method

Fig. 4.7 Clinical image example of brain tumor patient and nasopharyngeal cancer patient



Clinical Evaluation

Reconstructed images of brain tumor and nasopharyngeal cancer patients scanned by CdTe-PET are shown in Fig. 4.7. CdTe-PET identified intratumoral heterogeneity and visualized the tumor's edge sharply for both cancers.

4.3.2 Performance Evaluation of CdTe-SPECT by Phantom Experiment and Clinical Study

4.3.2.1 Dual-Radionuclide Character-Shape Phantom

The photopeaks of Tc-99m and I-123 were clearly discriminated in the measured energy spectrum (Fig. 4.8). The energy resolution of the CdTe semiconductor detector was high enough to separate the photopeaks of Tc-99m and I-123. The scatter-corrected images of Tc-99m and I-123 were clearly discriminated in the character-shape phantom image in Fig. 4.9. Because of the high-energy resolution of the CdTe semiconductor detector, there was no Tc-99m contamination in the I-123 window image even without scatter correction. The results suggested that simultaneous Tc-99m and I-123 study by using CdTe-SPECT was feasible.

4.3.2.2 Simultaneous Dual-Radionuclide Human Brain Study

The result of a simultaneous Tc-99m and I-123 dual-radionuclide scan is shown in Fig. 4.10. The Tc-99m HSAD and I-123 IMP images were clearly discriminated. The result suggests that CdTe-SPECT has the potential to produce accurate brain

Fig. 4.8 Energy spectrum of dual-radionuclide character-shape phantom measurement

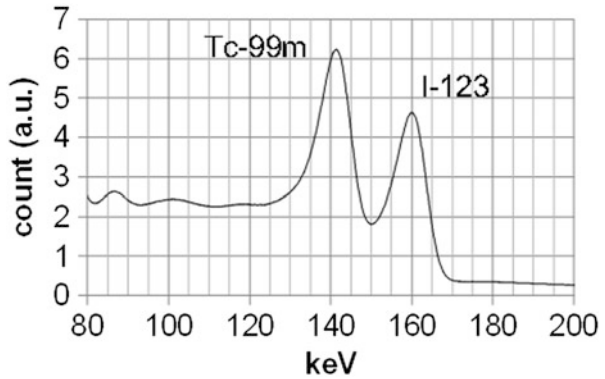


Fig. 4.9 Reconstructed image of dual-radionuclide character-shape phantom

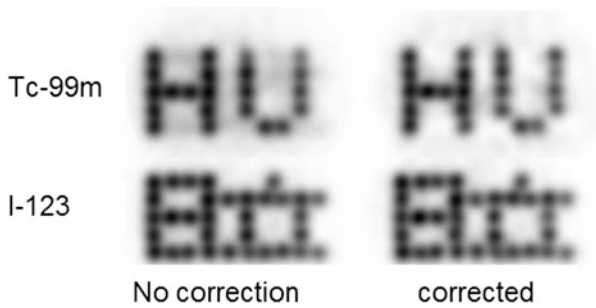
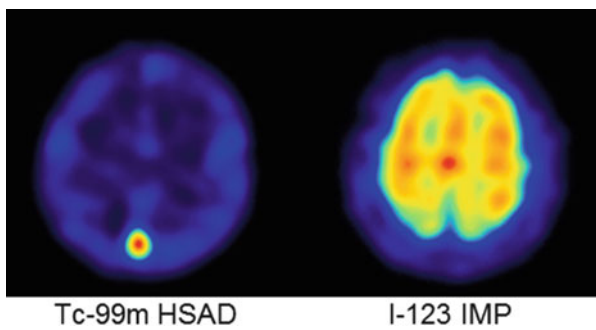


Fig. 4.10 Reconstructed image of simultaneous dual-radionuclide brain study



perfusion images (Tc-99m HSAD) and cerebral blood volume (Tc-99m HSAD) images simultaneously.

4.4 Conclusion

Prototype CdTe-PET and CdTe-SPECT systems were developed, and their performances were evaluated. The results suggest that CdTe-PET enables better identification of intratumoral metabolic distribution and that CdTe-SPECT will enable

simultaneous dual-radionuclide brain study to become available clinically. Semiconductor detectors have the potential to play a significant role in the future of nuclear medicine.

Acknowledgments This work was supported in part by the Creation of Innovation Centers for Advanced Interdisciplinary Research Areas Program, Ministry of Education, Culture, Sports, Science and Technology, Japan.

Open Access This chapter is distributed under the terms of the Creative Commons Attribution-Noncommercial 2.5 License (<http://creativecommons.org/licenses/by-nc/2.5/>) which permits any noncommercial use, distribution, and reproduction in any medium, provided the original author(s) and source are credited.

The images or other third party material in this chapter are included in the work's Creative Commons license, unless indicated otherwise in the credit line; if such material is not included in the work's Creative Commons license and the respective action is not permitted by statutory regulation, users will need to obtain permission from the license holder to duplicate, adapt or reproduce the material.

References

1. Morimoto Y, Ueno Y, Takeuchi W, Kojima S, Matsuzaki K, Ishitsu T, et al. Development of a 3D brain PET scanner using CdTe semiconductor detectors and its first clinical application. *IEEE Trans Nucl Sci.* 2011;58:2181–9.
2. Shiga T, Morimoto Y, Kubo N, Katoh C, Takeuchi W, Usui R, et al. A new PET scanner with semiconductor detectors enables better identification of intratumoral inhomogeneity. *J Nucl Med.* 2009;50:148–55.
3. Kubo N, Zhao S, Fujiki Y, Kinda A, Motomura N, Katoh C, et al. Evaluating performance of a pixel array semiconductor SPECT system for small animal imaging. *Ann Nucl Med.* 2005;19:633–9.
4. Bocher M, Blevis IM, Tsukerman L, Shrem Y, Kovalski G, Volokh L. A fast cardiac gamma camera with dynamic SPECT capabilities: design, system validation and future potential. *Eur J Nucl Med Mol Imaging.* 2010;37:1887–902.
5. Ko T, Utanohara Y, Suzuki Y, Kurihara M, Iguchi N, Umemura J, et al. A preliminary feasibility study of simultaneous dual-isotope imaging with a solid-state dedicated cardiac camera for evaluating myocardial perfusion and fatty acid metabolism. *Heart Vessel.* 2014. doi:10.1007/s00380-014-0578-4.
6. Suzuki A, Takeuchi W, Ishitsu T, Tsuchiya K, Ueno Y, Kobashi K. A four-pixel matched collimator for high-sensitivity SPECT imaging. *Phys Med Biol.* 2013;58:2199–217.
7. Suzuki A, Takeuchi W, Ishitsu T, Tsuchiya K, Morimoto Y, Ueno Y, et al. High-sensitivity brain SPECT system using cadmium telluride (CdTe) solid-state detector and 4-pixel matched collimator. *Phys Med Biol.* 2013;58:7715–31.
8. Seino T, Kominami S, Ueno Y, Amemiya K. Pulsed bias voltage shutdown to suppress the polarization effect for a CdTe radiation detector. *IEEE Trans Nucl Sci.* 2008;55:2770–4.
9. Tsuchiya K, Takahashi I, Kawaguchi T, Yokoi K, Morimoto Y, Ishitsu T, et al. Basic performance and stability of a CdTe solid-state detector panel. *Ann Nucl Med.* 2010;24:301–11.
10. Takeuchi W, Morimoto Y, Suzuki A, Matsuzaki K, Kojima S, Kobashi K, et al. Iterative reconstruction method using prior information and point spread function for high resolution CdTe PET scanner. *J Nucl Med(Meeting abstract).* 2008;49:388.

11. Green PJ. Bayesian reconstructions from emission tomography data using a modified EM algorithm. *IEEE Trans Med Imaging*. 1990;9:84–93.
12. Alenius S, Ruotsalainen U. Generalization of median root prior reconstruction. *IEEE Trans Med Imaging*. 2002;21:1413–20.
13. Reader AJ, Julyan PJ, Williams H, Hastings DL, Zweit J. EM algorithm system modeling by image-space techniques for PET reconstruction. *IEEE Trans Nucl Sci*. 2003;50:1392–7.
14. Panin VY, Kehren F, Michel C, Casey M. Fully 3-D PET reconstruction with system matrix derived from point source measurements. *IEEE Trans Med Imaging*. 2006;25:907–21.
15. Zaidi H. *Quantitative analysis in nuclear medicine imaging*. New York: Springer; 2006. p. 167–204.
16. NEMA. *NEMA standards publication NU2-1994*. 1994.
17. Ichihara T, Ogawa K, Motomura N, Kubo A, Hashimoto S. Compton scatter compensation using the triple-energy window method for single- and dual-isotope SPECT. *J Nucl Med*. 1993;34:2216–21.